Vibrational Spectroscopy of Water in Narrow Nanopores

ARTICLE *in* THE JOURNAL OF PHYSICAL CHEMISTRY B · MAY 2011

Impact Factor: 3.3 · DOI: 10.1021/jp109037q · Source: PubMed

2 AUTHORS, INCLUDING:

Christoph Dellago
University of Vienna
150 PUBLICATIONS **5,949** CITATIONS

SEE PROFILE

THE JOURNAL OF PHYSICAL CHEMISTRY B

ARTICLE

pubs.acs.org/JPCB

Vibrational Spectroscopy of Water in Narrow Nanopores

Marcus Weinwurm and Christoph Dellago*

Faculty of Physics, University of Vienna, Boltzmanngasse 5, 1090 Vienna, Austria

ABSTRACT: Inside narrow pores, for instance, realized as carbon nanotubes, water forms structures that strongly differ from the structure of bulk liquid water or ice. Here we compute vibrational spectra of such systems using molecular dynamics simulation combined with quantum mechanical perturbation theory. We focus on the spectroscopic response of single-file water chains in pores with subnanometer diameter, finding characteristic signatures of dangling and hydrogen-bonded hydrogen configurations occurring in this particular form of water. These features in the absorption spectra permit us to distinguish single-file water from the stacked-ring structures that form in wider pores. As previously observed in bulk liquid water, the vibrational frequency of the OH stretch of an HDO molecule in a system of D_2O molecules is essentially determined by the electric field acting at the position of the hydrogen atom, providing a way to link the spectroscopic response to the local charge distribution of specific molecular arrangements.

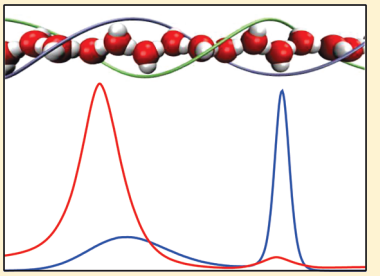

I. INTRODUCTION

As observed in computer simulations[1] and confirmed in recent experiments,[2] water fills the cavity of carbon nanotubes with diameters down to subnanometer widths. In such narrow pores, water forms ordered single-file chains of hydrogen-bonded molecules, as shown in Figure 1, that lie at the heart of several intriguing properties of such systems. Because of their 1D structure and the smoothness of the carbon nanotube walls, water chains support flow rates that exceed the expectations of macroscopic hydrodynamics by orders of magnitude.[3,4] At the same time, water wires in narrow pores provide routes for fast proton transport with diffusion constants about 40 times larger than that of bulk water.[5] In wider carbon nanotubes with diameters larger than 1 nm, water molecules form cylindrical structures consisting of polygonal water rings with antiferroelectric-like order.[6,7] Because of their unique properties, carbon nanotube membranes are promising building blocks for future filtration devices and hydrogen fuel cells[8,9] as well as model systems for biological transmembrane transport of ions and water.[10,11]

To date, the intriguing structural and dynamical properties of nanopore water have been explored mainly by computer simulation,[12] and experimental verification of single-file structures is still lacking. Whereas the experiments of Cambré et al.[2] convincingly demonstrate, through analysis of the radial breathing mode in Raman spectra, that carbon nanotubes fill down to a chiral index of (5,3), corresponding to a diameter of ∼0.55 nm, they do not probe the specific structure and dynamics of nanopore water. Similarly, density gradient centrifugation experiments indicate that carbon nanotubes with subnanometer diameters fill with water without yielding information on molecular arrangements.[13,14] Recently, we have suggested that dielectric spectroscopy may be used to accomplish this goal.[15−17] Calculations based on a simplified 1D dipole model, which accurately captures the free energetics of nanopore water,[18] reveal that the dielectric response of single file water to a homogeneous electric field in the direction of the pore axis carries characteristic signatures of the hydrogen-bonding defects that destroy the dipolar order of long water wires.[15] Detection of these signatures would yield unambiguous proof of the single-file structure of water in very narrow pores. Moreover, the excitation energy, the diffusion constant, as well as the effective interaction of hydrogen bonding defects can be extracted from such experiments.

In the present Article, we explore the possibility of detecting single-file structures with vibrational spectroscopy. Using a mixed quantum/classical approach recently devised by Eaves, Tokmakoff, and Geissler[19] combined with recent results of Skinner and collaborators,[20−23] we compute the infrared line shape of the OH stretching mode of an HDO molecule in a chain of D_2O molecules. The procedure is based on an almost linear relation between the frequency of the OH stretch and the electric field acting on the hydrogen atom,[20,21,24] such that the shape of the OH absorption band can be determined accurately from electric field distributions calculated in simulations using rigid water molecules modeled with an empirical force field.[25] Because the OH stretch is a sensitive probe of the local environment of the HDO molecule, its vibrational frequency discerns between the configuration in which the hydrogen atom is involved in a hydrogen bond to the next neighbor in the chain and the configuration in which the hydrogen atom is dangling. As a consequence, the vibrational spectrum of the OH stretch develops a bimodal shape that strongly differs from the infrared spectrum of bulk water. Because the spectrum of single-file water also differs from that of water confined to wider pores with more complex hydrogen bond topologies,[26] vibrational spectroscopy

Special Issue: Shaul Mukamel Festschrift

Received: September 21, 2010
Revised: December 16, 2010

   dx.doi.org/10.1021/jp109037q | J. Phys. Chem. B XXXX, XXX, 000–000

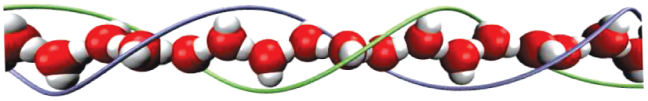

Figure 1. Single-file water chain in the interior of a narrow carbon nanotube (nanotube not shown). At low temperatures, the chain develops a helical structure, as indicated by the two spirals connecting the dangling hydrogen atoms of second nearest neighbors.

of the OH stretch provides a clear route for the experimental detection of single file water chains inside narrow pores.

The remainder of this article is organized as follows. In Section II, we outline the theoretical and computational methods used in this work. Vibrational spectra of a single-file water chain and of more involved water structures in wider carbon nanotubes are presented and discussed in Section III. Some concluding remarks are provided in Section IV.

II. THEORY AND SIMULATION METHODOLOGY

To determine the vibrational frequency the OH stretch of an HDO molecule in a chain of D_2O molecules, we follow the computational strategy of Eaves, Tokmakoff, and Geissler,[19] who modeled the OH vibration in liquid water as a 1D quantum-mechanical oscillator immersed in a bath of classical rigid water molecules. In the liquid, but also in the 1D water chain studied in the present work, the use of a 1D oscillator is justified because in the HOD molecule, intramolecular couplings are smaller than those to the surrounding water molecules.[27] The rigid water molecules evolve according to Newton's equation of motion, rotating and translating freely under the influence of forces determined from an empirical water model. For completeness, we reiterate the method of Eaves, Tokmakoff, and Geissler[19] in this section, closely following their notation.

A. Vibrational Frequencies. The Hamiltonian of the entire system can be written as a sum of three terms

$$H = H_s(P,Q) + H_{sb}(p,q,P,Q) + H_b(p,q) \qquad (1)$$

where Q and P are the position and momentum of the OH oscillator and q and p represent positions and momenta of the water molecules. In the above equation, $H_s(P,Q)$ is the Hamiltonian of the local vibrational mode, $H_b(p,q)$ is the energy of the classical part of the system governing its time evolution, and the system-bath Hamiltonian $H_{sb}(p,q,P,Q)$ couples the vibrational mode to the surrounding water molecules, that is, the bath molecules. The OH mode is represented by a Morse oscillator

$$H_s(P,Q) = \frac{P^2}{2\mu} + d[1-\exp(-aQ)]^2 \qquad (2)$$

where $\mu = m_H m_O/(m_H + m_O)$ is the reduced mass of the oxygen and the hydrogen atom, Q is the internal vibration coordinate, and $a = 2.13498$ Å^{-1} and $d = 549.0586$ kJ/mol are parameters of the Morse potential determining its width and depth.[27] The eigenfunctions of the Morse Hamiltonian can be expressed in terms of Laguerre polynomials such that the matrix elements of Q and Q^2, needed for the perturbative calculation of the vibrational frequencies, can be easily computed by numerical integration.[28]

The Morse oscillator is coupled to its environment through the system-bath Hamiltonian $H_{sb}(p,q,P,Q)$ arising from the interactions of the hydrogen and oxygen atoms of the OH oscillator with the bath molecules, as described by the empirical water model. Because the motion of the bath molecules is slow on the time scale of the OH vibration, the adiabatic approximation is valid, in which the bath variables are assumed to be fixed and the total Hamiltonian is considered to be a function of the vibrational coordinate only for the calculation of the instantaneous vibrational frequencies. As a further approximation, the system-bath Hamiltonian is expanded into a Taylor series in the vibrational coordinate Q and truncated after the quadratic term

$$H_{sb}(p,q,P,Q) = \frac{\partial V}{\partial Q}Q + \frac{1}{2}\frac{\partial^2 V}{\partial Q^2}Q^2 = FQ + GQ^2 \qquad (3)$$

Here F and G are the first and second derivatives of the interaction energy V with respect to the vibrational variable $Q = |\mathbf{r}_O - \mathbf{r}_H| - Q_0$, with the bath molecules fixed at their particular positions. Here $\mathbf{r}_O$ and $\mathbf{r}_H$ are the positions of the oxygen and hydrogen atom forming the OH oscillator, respectively, and Q_0 is the equilibrium length of the OH bond. These derivatives are evaluated at $Q = 0$, corresponding to the equilibrium length of the OH bond. An explicit expression for F can be derived by changing to the center of mass and relative coordinates[19]

$$F = \frac{\partial V}{\partial Q} = -\mu\hat{\mathbf{r}}_{OH}\cdot\left(\frac{\mathbf{F}_O}{m_O} - \frac{\mathbf{F}_H}{m_H}\right) \qquad (4)$$

where $\mu = m_O m_H/(m_O + m_H)$ is the reduced mass, $\hat{\mathbf{r}}_{OH} = (\mathbf{r}_O - \mathbf{r}_H)/|\mathbf{r}_O - \mathbf{r}_H|$ is the unit vector in direction from the H to the O atom, and the dot indicates a scalar product. The forces $\mathbf{F}_O$ and $\mathbf{F}_H$ are the total forces acting on the O and H atom, respectively, due to the interactions with all molecules of the system for a particular configuration. These forces follow from the empirical water model employed in the molecular dynamics simulation and are calculated to determine the time evolution of the system such that no extra computational cost is required for the calculation of F. Because the forces on the oxygen atom are comparable to those on the hydrogen atom, but the oxygen atom is much heavier than the hydrogen atom, the factor F is mainly determined by the force on the hydrogen atom, which, in typical empirical water models, is purely electrostatic in nature, such that one obtains the approximation

$$F \approx z_H\hat{\mathbf{r}}_{OH}\cdot\mathbf{E} \qquad (5)$$

Here $\mathbf{E}$ is the electric field at the hydrogen position and z_H is the charge of the H atom. Therefore, to first order, the frequency modulation of the OH oscillator due to interactions with the bath molecules is mainly mediated by the electric field acting at the hydrogen position in the bond direction.

The second derivative G of the total energy with respect to the oscillator variable can be calculated in a similar way by applying the chain rule to take into account the transformation from Cartesian to internal coordinates.[19] Again, exploiting the fact that the oxygen atom is much heavier than the hydrogen atom, one obtains

$$G = \frac{1}{2}\frac{\partial^2 V}{\partial Q^2} \approx -\frac{\mu^2 z_H}{2m_H}\hat{\mathbf{r}}_{OH}\hat{\mathbf{r}}_{OH}:\nabla_H\mathbf{E} \qquad (6)$$

where $\nabla_H\mathbf{E}$ is the tensor of the partial derivative of the electric field components with respect to the coordinates of the hydrogen atom and : denotes the tensor contraction. Therefore, the calculation of G requires the derivatives of the electric field $\mathbf{E}$ at the hydrogen position, quantities that are usually not calculated in a straightforward molecular dynamics calculation but that can be determined easily.

dx.doi.org/10.1021/jp109037q | J. Phys. Chem. B XXXX, XXX, 000–000

Using the expressions for F and G given above, one can calculate the vibrational frequency of the OH oscillator for fixed positions q of the bath molecules, which are assumed to be slowly varying function of time t. Solving the time-independent Schrödinger equation

$$(H_s + H_{sb})|\Psi[q(t)]\rangle = E_n[q(t)]|\Psi[q(t)]\rangle \quad (7)$$

yields the energies $E_n[q(t)]$ of the perturbed oscillator related to the fundamental frequency of the OH mode by

$$\hbar\omega_{OH}(t) = E_1[q(t)] - E_0[q(t)] \quad (8)$$

The notation used in the equations above emphasizes the fact that the energies and states of the perturbed oscillators are functions of time due to their parametric dependence on the positions $q(t)$ of the bath molecules that change in time. The energies $E_1[q(t)]$ can be easily determined by perturbation theory and to second order one obtains

$$E_n[q(t)] = \langle n|H_{sb}|n\rangle + \sum_{k\neq n} \frac{|\langle n|H_{sb}|k\rangle|^2}{e_n - e_k} \quad (9)$$

where $|n\rangle$ and e_n are eigenstates and eigenenergies of the unperturbed oscillator, respectively. Because typically the second-order term is considerably smaller than the first-order term, it can be neglected. In this approximation and also neglecting the term depending on G in eq 3, the vibrational frequency ω_{OH} is a linear function of the electric field at the hydrogen atom in direction of the OH bond

$$\hbar\Delta\omega_{OH} = z_H E_H(\langle 1|Q|1\rangle - \langle 0|Q|0\rangle) \quad (10)$$

where $\Delta\omega_{OH}$ is the frequency shift with respect to the gas phase frequency ω_0, that is, the frequency of the unperturbed Morse oscillator. For the parameters used in this Article, this frequency is $\omega_0/2\pi c = 3695\ \mathrm{cm}^{-1}$. In the above equation

$$E_H = \hat{\mathbf{r}}_{OH}\cdot\mathbf{E} \quad (11)$$

is the electric field acting at the position of the hydrogen atom in direction of the OH bond. Note that a negative E_H corresponds to a field pointing away from the oxygen atom to which the hydrogen atom is bonded. Eaves, Tokmakoff, and Geissler confirmed the accuracy of this approximate result for bulk water and used it to clarify the signature of hydrogen bonding in the vibrational spectroscopy of water.[19]

B. Infrared Line Shape. The computational procedure of Eaves, Tokmakoff, and Geissler[19] can also be used to compute the line shape for infrared absorption. The absorption spectrum is essentially given by the Fourier transform of the quantum dipole time correlation function[29,30]

$$\sigma(\omega) \propto \omega \int_{-\infty}^{+\infty} dt\, \exp(i\omega t)\langle \mu(0)\cdot\mu(t)\rangle \quad (12)$$

Here μ is the dipole operator of the OH oscillator and the angular brackets $\langle\cdots\rangle$ denote a time average. In the pure dephasing approximation, which is valid if the perturbation is so small that no transitions between the unperturbed states are induced, and neglecting states other than 0 and 1, one obtains[19]

$$\sigma(\omega) \propto \omega \int_{-\infty}^{\infty} dt\, e^{i\omega t}\langle \exp(-i/\hbar \int_0^t dt'[E_1(t') - E_0(t')])\rangle \times \langle \hat{\mathbf{r}}_{OH}(t)\cdot\hat{\mathbf{r}}_{OH}(0)\rangle e^{-|t|/2T_1} \quad (13)$$

Here the exponential factor takes into account the finite vibrational lifetime T_1 of the first excited state of the OH oscillator, and it is assumed that the transition dipole is in direction of OH bond.[20,31]

The expression for the infrared spectrum of eq 13 neglects correlations between the frequency fluctuations and the rotations of the HOD molecule, that is, changes of the direction of $\hat{\mathbf{r}}_{OH}$. Whereas this approximation may be reasonably accurate in the bulk, in a single-file chain of water molecules, the rotational behavior of the hydrogen-bonded and the dangling OH oscillator differs greatly (Section III), such that one needs to take into account orientational dynamics in this case

$$\sigma(\omega) \propto \omega \int_{-\infty}^{\infty} dt\, e^{i\omega t}\langle \exp(-i/\hbar \int_0^t dt'\,[E_1(t') - E_0(t')]) \times \hat{\mathbf{r}}_{OH}(t)\cdot\hat{\mathbf{r}}_{OH}(0)\rangle e^{-|t|/2T_1} \quad (14)$$

Another important effect neglected in eq 13 (and also in eq 14) is the dependence of the magnitude of the transition dipole on the local environment. Such non-Condon effects have been shown to affect importantly the IR spectra of bulk water,[32] and they are expected to play an even more pronounced role in single-file chains, where the local configurations available to the OH oscillator vary more strongly than those in the bulk. Taking into account non-Condon effects, the IR spectrum can be written as[20,32]

$$\sigma(\omega) \propto \omega \int_{-\infty}^{\infty} dt\, e^{i\omega t}\langle \exp(-i/\hbar \int_0^t dt'[E_1(t') - E_0(t')]) \times \mu_{10}(t)\cdot\mu_{10}(0)\rangle e^{-|t|/2T_1} \quad (15)$$

where

$$\mu_{01}(t) = \mu'(t)Q_{10}(t)\hat{\mathbf{r}}_{OH}(t) \quad (16)$$

is the matrix element of the dipole operator. Here $Q_{10}(t)$ is the matrix element of the vibrational variable between the vibrational ground and first excited state at time t, $\mu'(t)$ is the dipole derivative[20] at time t, and the dipole moment is taken in direction of the unit vector $\hat{\mathbf{r}}_{OH}(t)$ along the OH bond.

Both the matrix element $Q_{10}(t)$ and the dipole derivative $\mu'(t)$ are functions of the local configuration around the OH bond and, hence, are functions of time due to the dynamics of the system. Because these quantities cannot be determined within the theory outlined above, we take into account their configuration dependence through the empirical expressions determined by Skinner and collaborators based on electronic structure calculations,[20,21] which relate the matrix element Q_{10} to the instantaneous vibrational frequency ω_{OH}

$$Q_{10} = 0.1024\ \text{Å} - 0.927 \times 10^{-5}\ \text{Å/cm}^{-1}\omega_{OH} \quad (17)$$

and the dipole derivative μ' to the electric field E_H acting at the hydrogen position

$$\mu'/\mu'_g = 0.71116 - 1.470\ \text{V}^{-1}\ \text{Å}E_H \quad (18)$$

In the last equation, μ'_g is the dipole derivative in the gas phase. Note that in this Article we use the parametrization of ref 21 obtained from SPC/E water. These relations have been successfully

dx.doi.org/10.1021/jp109037q | J. Phys. Chem. B XXXX, XXX, 000–000

used to reproduce the main features of the IR spectra of HDO in liquid D_2O and D_2O ice.[20−22,33] In the following section, we present IR spectra of single-file water calculated from eqs 13−15 and compare them to assess the importance of the various approximations used to derive these equations.

In evaluating the expressions above for the IR spectrum, we use a vibrational lifetime of T_1 = 700 fs, as obtained for HDO in bulk D_2O in recent pump−probe experiments.[34,35] Because the main pathway for vibrational relaxation of the OH stretch is intramolecular in nature,[35] the use of this number extracted from bulk measurements is also justified for the 1D chain. For very short excitation lifetimes, the variation in the energies increases because of the uncertainty relation between energy and time, leading to line broadening. We neglect this effect in our calculations because the vibrational lifetime T_1 of the OH bond is too long to have an appreciable effect on the energies.[34,35]

C. Molecular Dynamics Simulation. In our molecular dynamics simulations, we integrated Newton's equations of motion using the velocity Verlet algorithm[36] with a time step of Δt = 1.7 fs at an energy corresponding to a temperature of 295 K in all cases. Water molecules interact via the SPC/E model[37] consisting of electrostatic interactions of charges placed at the oxygen and hydrogen positions and Lennard-Jones interactions with centers at the oxygen positions. The charges on the hydrogen and oxygen atoms are $z_O = -0.8476e$ and $z_H = 0.4238e$, respectively. Molecules are kept rigid with the RATTLE algorithm.[38] Periodic boundary conditions applied in the direction of the cylinder axis and electrostatic interactions of the periodic system were calculated with a rapidly converging 1D lattice sum.[39]

The single-file system consisted of one single HOD molecule and 30 D_2O molecules confined in the interior of a (6,6) carbon nanotube with a diameter of 8.1 Å, measured as the distance between carbon atoms on opposite sides of the CNT. The nanotube was not modeled with atomistic resolution but rather replaced by a cylindrically symmetric potential acting on the oxygen atoms with polynomial dependence on the oxygen-axis distance r

$$V_{sf}(r) = a_2 r^2 + a_4 r^4 + a_6 r^6 + a_8 r^8 \qquad (19)$$

with parameters $a_2 = -0.2281$ kcal mol^{-1} Å^{-2}, $a_4 = 1.09$ kcal mol^{-1} Å^{-4}, $a_6 = 0.2341$ kcal mol^{-1} Å^{-6}, and $a_8 = 0.3254$ kcal mol^{-1} Å^{-8}. This polynomial potential was extracted in a previous work from the radial density profile of a single water molecule inside a rigid and periodically replicated (6,6) carbon nanotube.[5] The length of the pore L was adjusted to yield a linear particle density $\rho = N/L = 0.385$ Å^{-1}, as calculated by Striolo, Chialvo, and Gubbins for a (6,6) carbon nanotube in contact with a water bath under ambient conditions.[40] The same interaction of the water molecules with the CNT walls was used also for the wider carbon nanotubes. In this case, however, the potential acted on the oxygen atoms only beyond a certain distance r_0 from the pore axis

$$V_w(r) = \begin{cases} 0 & \text{for} \quad r \le r_0 \\ V_{sf}(r - r_0) & \text{for} \quad r > r_0 \end{cases} \qquad (20)$$

For the wider carbon nanotubes, the radius r_0 was selected such that the diameter $d = d_{(6,6)} + 2r_0$ corresponds to the systems studied in ref 41. Here $d_{(6,6)}$ is the diameter of the (6,6) nanotube. The parameters of our simulations are summarized in Table 1. We have verified that for these parameters the water structures forming in our molecular dynamics simulations, discussed in detail in Section IIB, are the same as those of ref 41. The time evolution of the nanopore water was followed for 34 ns for the single file case and for 204 ns for the water in the wider pores.

Table 1. Parameters of the Molecular Dynamics Simulations from Left to Right: Type of Carbon Nanotube, Number N of Water Molecules (Including the HDO Molecule), Diameter d, System Length L, Linear Density $\rho = N/L$, Morphology of the Structure That Forms in the Pore (See Section IIIB)

CNT	N	d [Å]	L [Å]	ρ [Å^{-1}]	structure
(6,6)	31	8.1	80.5	0.385	single-file
(8,8)	120	10.9	85.1	1.410	tetragonal
(9,8)	150	11.5	89.3	1.680	pentagonal
(9,9)	180	12.2	93.3	1.930	hexagonal
(10,10)	200	13.6	95.0	2.105	disordered

D. Summary of the Computational Procedure. In summary, we calculate vibrational frequencies and IR spectra of the OH stretch of an HDO molecule in D_2O inside the pore of a nanotube with various diameters using the following procedure. Starting from an appropriately equilibrated configuration, we follow the time evolution of the system of rigid molecules with the velocity Verlet algorithm. After each time step, the energy and the vibrational frequency of the OH oscillator are calculated from first-order perturbation theory according to eqs 8 and 9. For this calculation, we need the matrix elements $\langle n|Q|n\rangle$ and $\langle n|Q^2|n\rangle$ of the two lowest energy eigenstates of the Morse oscillators. The values of the relevant matrix elements, computed by numerical integration using the known Morse eigenfunctions, are $\langle 0|Q|0\rangle$ = 0.01499 Å, $\langle 1|Q|1\rangle$ = 0.04604 Å, $\langle 0|Q^2|0\rangle$ = 0.00498 Å^2, and $\langle 1|Q^2|1\rangle$ = 0.01661 Å^2. The calculation of the vibrational frequency also requires the computation of the expansion coefficients F and G, which depend on the particular configuration of the system. Whereas we calculate F exactly according to eq 4 from the total forces acting on the O and H atoms of the HOD molecule, we determine G approximatively using eq 6. By collecting statistics along the integrated trajectory, we determine frequency and electric field distributions. Note that representing the OH stretch vibration as quantum mechanical oscillator has no influence on the time evolution of the HDO and D_2O molecules, which is governed exclusively by the classical equations of motion.

Besides collecting this purely static information, we also compute correlation functions, such as the frequency correlation function $C_{\omega\omega}(t) = \langle \omega_{OH}(0)\omega_{OH}(t)\rangle$, that probe the specific dynamics of the HOD molecule and the surrounding D_2O molecules. Following the system in time, we determine the orientational correlation function $\langle \hat{\mathbf{r}}_{OH}(t)\cdot\hat{\mathbf{r}}_{OH}(0)\rangle$ of the OH bond as well as the correlation function $\langle \exp[-(i/\hbar)\int_0^t dt' E_1(t') - E_0(t')]\rangle$, which depends on the time evolution of the energy difference of the two lowest-lying states. Fourier transformation of the product of these correlation functions including an appropriate damping factor according to eq 13 then yields the infrared absorption spectrum of the OH stretch. Similarly, we also compute the correlation functions of eqs 14 and 15, for which the environment dependence of the transition dipole is taken into account via the maps 17 and 18. Note that whereas quantities like the electric field distribution $P(E)$ are purely static and hence do not depend on the masses assigned to the atoms, the accurate calculation of time correlation functions requires us to consider one single HOD molecule interacting with D_2O molecules.

dx.doi.org/10.1021/jp109037q | J. Phys. Chem. B XXXX, XXX, 000–000

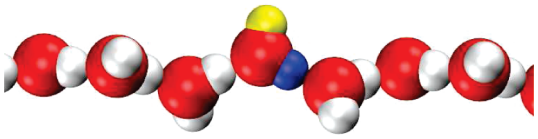

Figure 2. Hydrogen atoms of a water molecule in a single file chain can be in two different configurations, as indicated by the different colors of the hydrogen atoms of the central molecule. Whereas the hydrogen bonded hydrogen atom (blue) is involved in a hydrogen bond to the next water molecule in the chain, the dangling hydrogen atom (yellow) is not and experiences a greater configurational freedom.

III. RESULTS

A. Single-File Water. In a narrow carbon nanotube, water forms a 1D single-file chain, in which each molecule accepts one hydrogen bond from one neighboring molecule and donates one hydrogen bond to a molecule on the other side. In this particular structure, the dipole moments of all water molecules point approximately in the same direction (e.g., they all point to the right in Figure 1). Although such collective dipolar order cannot persist in the thermodynamic limit because of the local interactions of water molecules, single-file water chains are typically ordered over almost macroscopic distances because of the high energy required to generate the hydrogen bonding defects that destroy this order.[18] In the present Article, we consider only short chains, which are perfectly ordered almost all of the time. Such chains have two ordered states, with dipoles either parallel or antiparallel to the tube axis. Transitions between these states occur via a hydrogen-bonding defect that is created at one end of the chain, diffuses along the chain, and leaves it at the other side.[16,42] If the water chain experiences periodic boundary conditions (as do the chains considered here), then the dipoles of the chain only flip if a defect pair is created, the two defects diffuse in opposite directions, and eventually recombine. On the basis of previous results,[16] one can estimate that typical times for collective dipole reorientation of the water chain considered here are on the order of tens of microseconds. On the nanosecond time scale of our simulations, the flip of the whole chain is a very rare event, which we never observed. Hence, our chains have a given dipole direction that, up to small thermal fluctuations, does not change in time.

In the ordered chain, the hydrogen atoms of each water molecule occur in two distinct configurations. Either the hydrogen atom is involved in a hydrogen bond, we call this atom hydrogen-bonded, or it is not; then, we speak about the dangling hydrogen atom. These two different positions of the hydrogen/deuterium atom are indicated with different colors in Figure 2. We use the same terminology to specify the two different environments to which the OH bond can be exposed. As discussed in detail in the subsequent sections, the vibrational response of the OH oscillator is sensitive to the particular environment experienced by the hydrogen atom in the two distinct positions.

Because of the repulsive interaction of the dangling hydrogen atoms of subsequent water molecules in the chain, their dangling OH bonds tend to be oriented in a antiparallel fashion. To express this observation quantitatively, we define the azimutal angle φ_i of the dangling OH bond of water molecule i as

$$\varphi_i = \arctan[\hat{y}_{\mathrm{OH}}^{(i)}/\hat{x}_{\mathrm{OH}}^{(i)}] \tag{21}$$

Here $\hat{x}_{\mathrm{OH}}^{(i)}$ and $\hat{y}_{\mathrm{OH}}^{(i)}$ are the x and y components of the unit vector $\hat{\mathbf{r}}_{\mathrm{OH}}^{(i)}$ in the direction of the dangling OH bond of water molecule, i, respectively. The z-axis points in the direction of the pore axis, whereas the x and y axes are orthogonal to it. At high temperatures, the azimutal angles of neighboring molecules typically differ by π with thermal fluctuations around this value. As a consequence, the azimutal angle difference between second nearest neighbors approximately vanishes

$$\Delta\varphi_i = \varphi_{i+2} - \varphi_i \approx 0 \tag{22}$$

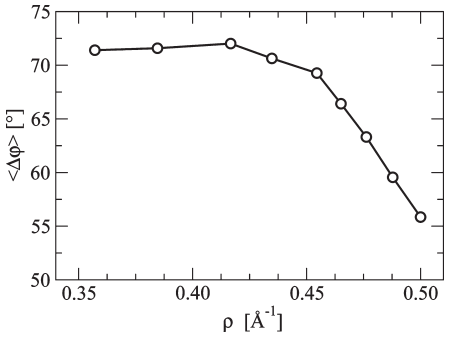

Figure 3. Difference $\Delta\varphi$ between the azimutal angle of second nearest neighbors as a function of the linear density $\rho = N/L$ for configurations corresponding to potential energy minima determined with simulated annealing. An angular difference deviating from zero is indicative of the helical structure of the water chain.

At lower temperatures, however, the water chain develops a helical structure, as shown in Figure 1. We obtained the configuration of the water chain shown in this Figure by minimizing the potential energy with a simulated annealing procedure. To avoid artifacts caused by the incommensurability of the winding number with the number of periodically replicated molecules, we have carried out this calculation without periodic boundary conditions. The helical structure of the water chain is also reflected in a second neighbor angular difference that differs from zero, $\Delta\varphi_i \neq 0$, as shown in Figure 3 for different linear densities ρ. At higher temperatures, the helical structure is destroyed by thermal fluctuations, and at room temperature, for instance, the dangling OH bond rotates quite freely around the pore axis while maintaining the tendency to point in the opposite direction of the dangling OH bonds of the neighboring water molecules.

On a picosecond time scale, the dynamics of the water chain is dominated by flips of individual water molecules, during which the dangling atom and the hydrogen-bonded atom interchange their role.[43] The transition occurs essentially through the rotation of the water molecule around the axis orthogonal to the molecular plane and involves the crossing of a barrier of a few $k_{\mathrm{B}}T$.[43] To analyze this type of motion, in which one hydrogen atom replaces the other one in the hydrogen bond to the next water molecule, we have calculated the hydrogen bonding correlation function $C_{\mathrm{hb}}(t)$ of the OH bond of the HDO molecule in a chain of D_2O molecules

$$C_{\mathrm{hb}}(t) = \langle \delta h(0)\delta h(t)\rangle \tag{23}$$

Here $\delta h(t) = h(t) - \langle h\rangle$ and $h(t)$ is an indicator function that is unity if the OH bond is hydrogen bonded and vanishes if the OH bond is dangling. A similar correlation function has been used to study the kinetics of hydrogen bond formation and cleavage in bulk liquid water[44,45] and in water clusters.[46] Because on the time scale of our simulations the water chain is always defect-free, the

dx.doi.org/10.1021/jp109037q |J. Phys. Chem. B XXXX, XXX, 000–000

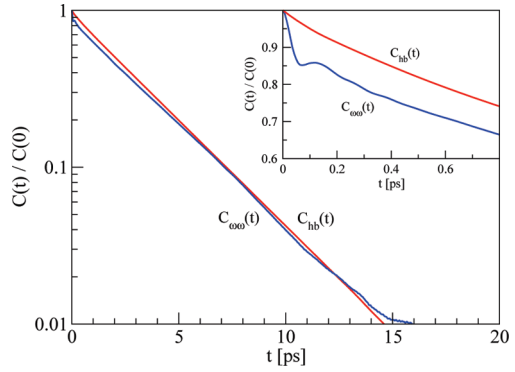

Figure 4. Frequency correlation function $C_{\omega\omega}(t)$ and hydrogen bond correlation function $C_{hb}(t)$ normalized by their respective values at $t = 0$. In the inset, the same correlation functions are displayed in the short time range with a linear scale on the y axis. Exponential fits in the time range with exponential decay yield a correlation time of about $\tau \approx 3.2$ ps in both cases.

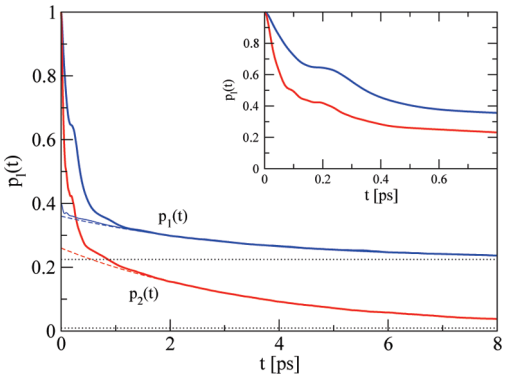

Figure 5. Angular correlation functions $p_1(t)$ and $p_2(t)$ (solid lines). The dotted lines represent the asymptotic values of the two functions, $\langle p_1(\infty)\rangle = 0.2245$ and $\langle p_2(\infty)\rangle = 0.00968$. The inset contains the same curves on a shorter time scale. For long times, $p_1(t)$ and $p_2(t)$ approach their asymptotic values exponentially with relaxation times of $\tau_1 \approx 3.3$ ps and $\tau_2 \approx 3.4$ ps, respectively. The fits to the exponential functions are shown as thin dashed lines. The correlation function does not decay to zero because on the time scale of our simulations the symmetry is broken and the water molecules are collectively oriented in one direction. The contribution to $p_1(t)$ arising from the z component of the unit vector r_{OH} is shown as a thin solid line. As can inferred from the Figure, this contribution is identical to the full correlation function $p_1(t)$ for all times $t > 1$ ps.

H or D atom of the HDO molecule that is closest to the oxygen atom of the next molecule in the chain is defined to be the hydrogen-bonded one, whereas the other is the dangling one. According to this definition, the HDO molecule has exactly one dangling H/D atom and one hydrogen bonded atom at all times. Because configurational properties do not depend on the masses of the atoms and the H and D atoms interact with neighboring water molecules in exactly the same way, the probability that the OH is hydrogen bonded is $\langle h\rangle = 1/2$. The hydrogen bonding correlation function $C_{hb}(t)$ is simply related to the conditional probability $P_{hb}(t) = \langle h(0)h(t)\rangle/\langle h\rangle$ that the OH bond is hydrogen bonded at time t given that it was hydrogen bonded at time 0, $P_{hb}(t)=2C_{hb}(t) + {}^1/_2$.

As shown in Figure 4, $C_{hb}(t)$ decays exponentially with a relaxation time of $\tau_{hb} \approx 3.2$ ps. Because the long time behavior of $C_{hb}(t)$ is insensitive to fleeting breakings of the hydrogen bond, this relaxation time can be considered to be the lifetime of the hydrogen bond. Interestingly, the time derivative of the hydrogen-bonding correlation function measured in our simulation does not display the oscillatory behavior observed for bulk water in the time range $t < 200$ fs.[44,45] This is most likely due to a difference in the hydrogen bond definitions. Whereas in our case, we assign the hydrogen bond to the hydrogen atom closest to the neighboring oxygen atom, a distance-angle criterion is commonly used in bulk simulations. In the latter case, hydrogen bonds can seemingly break but reform a short time later. These brief events, essentially absent in our simulations, determine the short-time behavior of the correlation function in the bulk.

Because the vibrational frequency of the OH bond is sensitive to the local environment, the switches of the H atom in and out of the hydrogen bond will importantly contribute to the decay of the frequency correlation function

$$C_{\omega\omega}(t) = \langle \delta\omega(0)\delta\omega(t)\rangle \tag{24}$$

where $\delta\omega(t) = \omega(t) - \langle\omega\rangle$ is the deviation of the instantaneous frequency $\omega(t)$ at time t from its time-averaged value, $\langle\omega\rangle$. Under certain simplifying assumptions, the vibrational third-order response can be expressed in terms of $C_{\omega\omega}(t)$.[30] Because this function can be determined experimentally, for instance, in vibrational echo peak shift measurements,[35,47] the frequency correlation function provides a convenient way to establish a link between simulation results and experimental data.

For single-file water, the frequency correlation function, shown in Figure 4, displays a fast short-time decay due to the librational motion of the HDO molecule, which then turns into an exponential decay with the same relaxation time as the hydrogen-bond correlation function. This exponential decay is a reflection of the two-state kinetics of the system with uncorrelated interconversions between the structures in which the OH bond experiences different surroundings.

The two-state behavior associated with the breaking and formation of hydrogen bonds also affects the long-time behavior of the orientational correlation functions of the transition dipole unit vector $\hat{\mathbf{r}}_{OH}$[43]

$$p_l(t) = \langle P_l[\hat{\mathbf{r}}_{OH}(0)\cdot\hat{\mathbf{r}}_{OH}(t)]\rangle \tag{25}$$

Here $P_l(x)$ is the lth Legendre polynomial such that for $l = 1$ and 2 one has

$$p_1(t) = \langle \hat{\mathbf{r}}_{OH}(0)\cdot\hat{\mathbf{r}}_{OH}(t)\rangle \tag{26}$$

and

$$p_2(t) = \frac{1}{2}\langle 3[\hat{\mathbf{r}}_{OH}(0)\cdot\hat{\mathbf{r}}_{OH}(t)]^2 - 1\rangle \tag{27}$$

respectively. These functions are important in the analysis of the dynamics because they can be determined experimentally.[34,35] Note that $p_1(t)$ is the orientational correlation function that enters in the calculation of the infrared spectrum according to eq 13. Both orientational correlation functions $p_1(t)$ and $p_2(t)$, shown in Figure 5, have a shoulder at 200 fs due to the librational motion of the water molecules. The rapid decay of $p_1(t)$ and $p_2(t)$ for $t < 1$ ps is due to the rotational diffusion of the dangling OH bond around the pore axis. In contrast, the long time decay is due to flips of the HDO molecule between its two possible states. This interpretation is confirmed by comparing the full time correlation function $p_1(t)$ to its contribution arising from the z

dx.doi.org/10.1021/jp109037q |J. Phys. Chem. B XXXX, XXX, 000–000

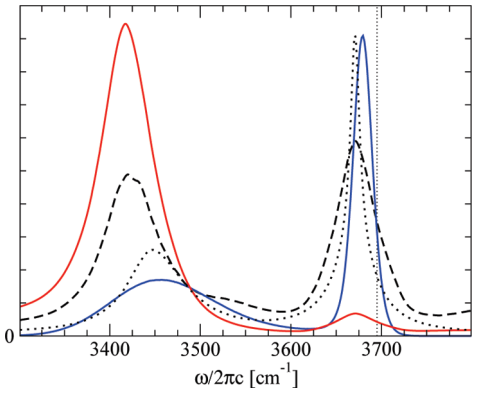

Figure 6. Distribution $P(\omega)$ of the OH stretch frequency (blue) and infrared spectrum $\sigma(\omega)$ (red) computed according to eq 15 for single-file water. Also included are spectra computed neglecting non-Condon effects with (dashed line, eq 14) and without (dotted line, eq 13) the inclusion of correlations between frequency fluctuations and molecular rotations. The vertical dotted line indicates the vibrational frequency of the unperturbed Morse oscillator, $\omega_0/2\pi c$ = 3695 cm^{-1} and arbitrary units apply on the vertical axis.

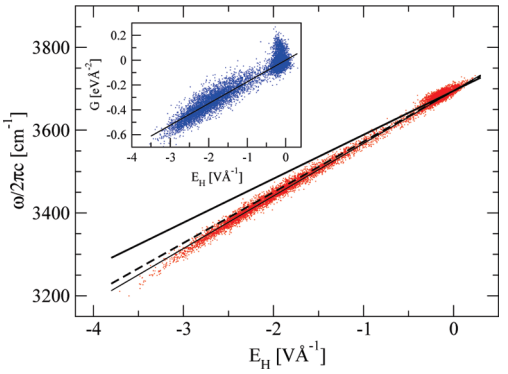

Figure 7. Scatter plot of frequency ω versus electric field E_H at the position of the hydrogen atom. A linear fit (thin solid line) with fixed $\omega_0/2\pi c$ = 3695 cm^{-1} through the 10 000 data points yields $\omega/2\pi c = \omega_0/2\pi c + aE_H$ with a = 127.0 cm^{-1} Å V^{-1}. The thick solid line with slope 106.14 cm^{-1} Å V^{-1} is the prediction of eq 10. The dashed line with slope 122.52 cm^{-1} Å V^{-1} includes contributions of the second-order term of the system-bath Hamiltonian, computed as described in the main text. Inset: Scatter plot of the second-order coefficient G versus the electric field E_H at the position of the hydrogen atom. The strong correlation between G and E_H contributes to the linear dependence of the frequency on the electric field. A linear fit to the 10 000 data points going through the origin (solid line) yields slope of 0.1746 e/Å.

component of the unit vector in OH direction. This contribution, shown as a dotted line in Figure 5, is essentially identical to the full correlation function for $t > 1$ ps, indicating that in this time regime contributions originating from the x and y components of the OH vector have already disappeared. These contributions, however, determine the short time behavior of the correlation function. For long times, the orientational correlation function decays exponentially with the same relaxation time as the hydrogen bonding correlation function and the frequency correlation function.

The two-state behavior is also apparent in the frequency distribution $P(\omega)$ of the OH stretch shown in Figure 6 together with the infrared spectrum $\sigma(\omega)$ calculated according to eq 15. Whereas the frequency distribution is a purely structural quantity that does not depend on dynamics, the infrared spectrum depends explicitly on the time evolution of the system. Nevertheless, both functions show qualitatively similar features. The frequency distribution has a high and narrow peak that is slightly red-shifted with respect to the gas-phase frequency and a broad peak with a stronger red shift. Whereas the narrow peak is due to configurations, in which the OH bond is dangling, the broad peak corresponds to situations where its hydrogen atom is bonded. Statistics collected separately for these two classes of configurations confirm this picture. In the hydrogen-bonded state, librational motion causes the OH bond to explore configurations that differ in the local atomic arrangements leading to a frequency distribution that is much broader than that of the dangling OH bond with a relatively uniform local environment. Note that the integrals of the frequency correlation function $P(\omega)$ over the low- and the high-frequency peaks are the same because as a result of symmetry, the dangling and hydrogen-bonded configurations of the OH bond are equally likely.

The height of the high-frequency peak of the IR spectrum is strongly reduced with respect to the frequency distribution mostly due to non-Condon effects, that is, the dependence of the transition dipole on the local environment. Because of the large difference in the electric field acting on the hydrogen atom in the hydrogen bonded and the dangling configuration, the magnitudes of the transition dipole of these two populations typically differ by a factor of about five[21] (eq 18), considerably suppressing the IR spectrum at higher frequencies. For comparison, we have included in Figure 6 also IR spectra calculated for single-file water neglecting such non-Condon effects. Whereas the spectrum shown as a dotted line was obtained from eq 13 assuming that frequency fluctuations are uncorrelated to the rotational motion of the HOD molecule, such correlations were taken into account for the spectrum shown as the dashed line computed according to eq 14. Clearly, both correlations and non-Condon effects play an important role in the IR spectrum of single-file water as they do in the case of bulk water.[32]

As discussed in Section II, the electric field E_H acting at the hydrogen position in direction of the OH bond is expected to be the major determinant for the shift of the vibrational frequency of the OH bond. In bulk water, the approximate linear relation between electric field and vibrational frequency was found to hold with high accuracy, providing an effective way to relate the vibrational response to specific molecular arrangements.[19] Not surprisingly, this linear relation is valid also for the OH bond of the HDO molecule in the single-file chain of D_2O molecules, as demonstrated in Figure 7. Fitting the (ω,E_H) pairs shown in Figure 7 using a straight line with offset $\omega_0/2\pi c$ = 3695 cm^{-1}, corresponding to the gas-phase frequency, one finds $\omega/2\pi c = \omega_0/2\pi c + aE_H$, where a = 127.0 cm^{-1} Å V^{-1}. All points of the scatter plot lie very close to this linear relationship, confirming the expectation that the vibrational frequency essentially depends only on the electric field E_H, as suggested by eq 10.

The proportionality factor in the linear relation between the frequency shift and the electric field as expressed in eq 10 can be easily calculated

$$\Delta\omega_{OH}^{F} = \frac{z_H(\langle 1|Q|1\rangle - \langle 0|Q|0\rangle)}{hc}E_H = \frac{106.14\ \text{cm}^{-1}}{\text{V/Å}}E_H \quad (28)$$

Here h is Planck's constant and the charge of the hydrogen atom is z_H = 0.4238e. The above expression, shown in Figure 7 as a

dx.doi.org/10.1021/jp109037q |J. Phys. Chem. B XXXX, XXX, 000–000

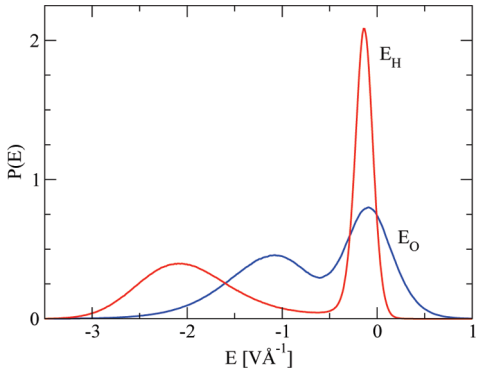

Figure 8. Distribution of the electric field in direction of the OH bond at the position of the hydrogen atom (E_H, red line) and at the position of the oxygen atom (E_O, blue line).

thick solid line, underestimates the magnitude of the frequency shift by ~15%. This discrepancy raises the question of which factors cause the deviation while still maintaining the linear relation between the frequency shift and the electric field. An answer can be found by analyzing the connection between the electric field E_H and G, the second-order term of the system-bath Hamiltonian. (See eq 3.) The scatter plot of (G,E_H) pairs, shown in the inset of Figure 7, indicates that G and E_H are strongly correlated and display an almost linear dependence on each other, such that the proportionality $G \approx bE_H$ holds with good accuracy. A linear fit to the simulation data yields $b = 0.1746\ e/\text{Å}$. Using this approximate relationship, the frequency shift due to the second-order coupling term is obtained as

$$\Delta\omega_{OH}^{G} = \frac{b(\langle 1|Q^2|1\rangle - \langle 0|Q^2|0\rangle)}{hc}E_H = \frac{16.38\ \text{cm}^{-1}}{\text{V/Å}}E_H \quad (29)$$

This contributions amounts to ~15% of $\Delta\omega_{OH}^{F}$. Together, $\Delta\omega_{OH}^{F}$ and $\Delta\omega_{OH}^{G}$ account for most of the frequency shift, as indicated by the dashed line in Figure 7.

Because of the approximate linear relationship between electric field and frequency, the form of the field distribution, shown in Figure 8, closely follows the bimodal shape of the frequency distribution. Both peaks carry equal statistical weight. The broad peak centered at $E_H \approx -2.1\ \text{V Å}^{-1}$ is essentially due to the electric field acting on the hydrogen atom in the hydrogen bonded position. The most significant contributions to this peak come from the Coulombic attraction between the hydrogen atom and the oxygen atom accepting the hydrogen bond. Note that a negative electric field pulls the hydrogen atom in the direction away from the oxygen atom to which it is bonded. Because as a result of the librations of the HOD molecule the field at the hydrogen atom changes in magnitude and direction, the peak on the red side is considerably broader than the narrow peak centered at the slightly negative field value of $E_H \approx -0.1\ \text{V Å}^{-1}$. This peak receives contributions mainly from configurations in which the OH bond is dangling, and the H atom interacts only weakly with charges located on other molecules. The negative charges located at the oxygen sites of the neighboring molecules attract the charge of the dangling hydrogen atom and pull it toward the pore axis, corresponding to a positive electric field E_H. Therefore, it is surprising to find the peak arising form dangling hydrogen configurations at negative rather than at positive fields. A closer analysis reveals that the combined effect of the deuterium charges on the neighboring molecules produces a negative field that compensates for the positive electric field generated by the oxygen charges. The largest contribution to this negative field comes from the deuterium atom involved in the hydrogen bond to the HOD molecule.

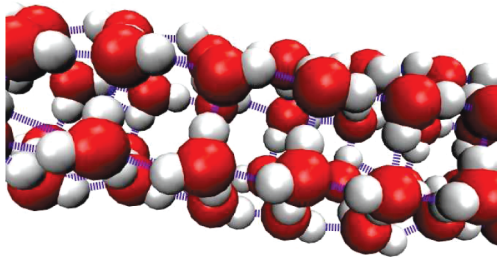

Figure 9. Hydrogen-bond network in a hexagonal water structure forming inside a (9,9) CNT. The hydrogen bonds are indicated by dashed blue lines.

Figure 8 also includes a plot of the distribution of the electric field E_O at the oxygen position of the HDO molecule. For both the dangling and hydrogen-bonded configuration, the oxygen atom stays in the same position such that the magnitude of the electric field at this position is essentially constant up to thermal fluctuations. Nevertheless, the electric field distribution $P(E_O)$ has two peaks, one at −0.05 V/Å associated with the dangling OH bond and one at −1.1 V/Å because of the hydrogen-bonded configuration. This bimodality arises because the direction, in which the electric field is determined, changes with the reorientation of the OH bond between the dangling and hydrogen-bonded configuration. Therefore, depending on the particular configuration of the hydrogen bond, E_O probes the electric field in the direction of the pore axis or orthogonal to it.

B. Water in Wide Carbon Nanotubes. To identify unambiguously single-file water in nanopores based on its spectroscopic signature, it is important to know the vibrational spectra of other, non-single-file structures that can form in narrow pores. Only if single-file and non-single file water structures differ in their spectroscopic response can one hope to distinguish various forms of nanopore water using vibrational spectroscopy. We have therefore also computed the frequency distributions and infrared absorption spectra for water confined in the cavity of slightly wider carbon nanotubes with diameters ranging from 10.9 to 13.6 Å. Under such confinements, which can be realized inside carbon nanotubes with chiral indices (8,8), (9,8), (9,9), and (10,10), ice-like structures form,[7,26,41,48] consisting of stacked rings of various numbers of molecules, as shown in the insets of Figure 10. Within each ring, water molecules are linked by intraring hydrogen bonds. Rings, in turn, are connected by inter-ring hydrogen bonds. Each water molecule donates and receives two hydrogen bonds and is involved in an equal number of intra- and inter-ring hydrogen bonds. As example, a side view of the hydrogen bond network of stacked six-membered rings inside a (9,9) CNT is shown in Figure 9. In the (10,10) CNT, the widest pore studied here, the water molecules form a structure of stacked seven-membered rings[48] at low temperatures but are disordered at the temperature of 295 K used in all of our simulations.

Although there are two distinct types of hydrogen bonds, inter-ring and intraring hydrogen bonds, the environments of the hydrogen atom are rather similar in both situations. Nevertheless, there are differences between the vibrational response of the OH bond in the intra- and inter-ring configurations. This effect, probably due to the curvature of the cylindrical water

dx.doi.org/10.1021/jp109037q |J. Phys. Chem. B XXXX, XXX, 000–000

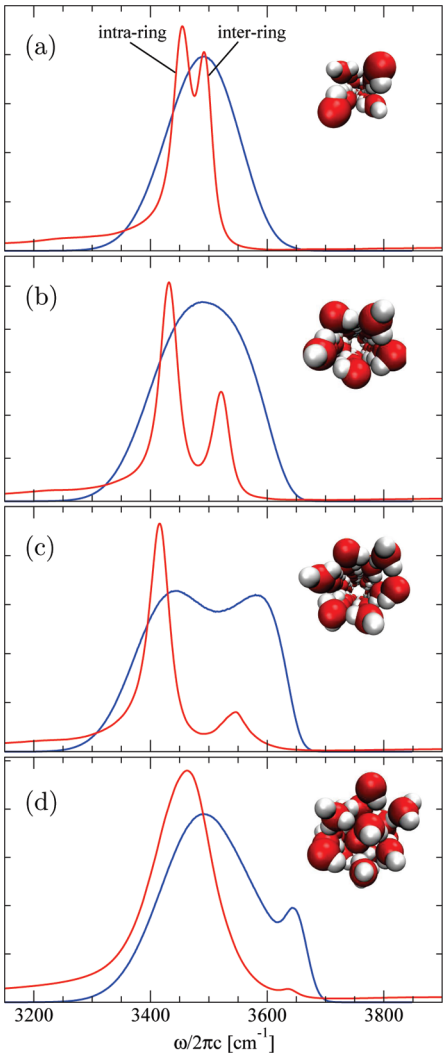

Figure 10. Frequency distributions (blue) and infrared spectra (red) of water inside carbon nanotubes with different chiral vectors (n,m). Arbitrary units are used on the y axis. (a) (8,8) CNT with tetragonal rings, (b) (9,8) CNT with pentagonal rings, (c) (9,9) CNT with hexagonal rings, and (d) (10,10) CNT with disordered water. In the infrared spectra of panels a−c, the high-frequency peak corresponds to the inter-ring hydrogen atom and the low-frequency peak to the intraring hydrogen atom. The insets show the water structures forming inside the cavity of the CNTs (view along the tube axis; CNTs not shown).

configurations, is clearly noticed in the infrared spectra of the tetragonal, pentagonal, and hexagonal structures, shown alongside with the corresponding frequency distributions in Figure 10a−c. These spectra were computed according to eq 15 including non-Condon effects, that is, the dependence of the transition dipole on the local molecular structure. These effects lead to a considerable suppression of the high-frequency part of the spectra.

For the tetragonal and pentagonal structures, the frequency distributions have a single peak, such that the instantaneous frequency ω does not discriminate between the two hydrogen configurations. For the hexagonal rings, a second peak appears on the blue side of the line. In all of these cases, the infrared spectra display two well distinct peaks separated by 30−80 cm^{-1}. By collecting statistics separately for the two hydrogen positions, we identified the high- and the low-frequency peaks as belonging to the inter-ring hydrogen atom and the intraring hydrogen atom, respectively. The splitting into two peaks arising in the IR spectra is due to motional narrowing, which is more pronounced for the ice-like structure in the wider CNTs than for single file water because of the slower decay of the orientational correlation function of the OH bond. For the tetragonal system, for instance, flipping of the OH bond between the inter-ring and intraring positions occurs on a time scale of roughly 100 ps. Therefore, the infrared spectrum shows a clear signature of the stacked-ring-structures of water in wider pores, whereas in the frequency distributions, the asymmetry of the hydrogen environments in the inter-ring and intraring configurations manifests itself less strongly. Similar spectra for nanopore water were obtained by Byl et al.[26] from molecular dynamics simulations using flexible water molecules. Compared with their results, however, our intraring peaks are blue-shifted by ∼60 cm^{-1}.

In contrast with the ordered structures discussed above, in which all hydrogen/deuterium atoms are involved in hydrogen bonds, dangling hydrogen atoms exist in the disordered liquid-like water forming in the (10,10) CNT at a temperature of 295 K. Under these conditions, the molecules diffuse freely through the system. The dangling hydrogen atoms lead to the small peak appearing at the blue side of both the frequency distribution and the infrared spectrum shown in Figure 10e. The broad low-frequency peak, on the other hand, is associated with hydrogen atoms involved in hydrogen bonds. Note that for the liquid-like structures in the (10,10) CNT, motional narrowing is less pronounced than that in the ice-like structures because of the fast decay of dipole−dipole correlations.

IV. CONCLUSIONS

Using classical molecular dynamics simulation combined with quantum mechanical perturbation theory, we have determined vibrational spectra for water confined in the interior of narrow carbon nanotubes. In these calculations, we considered the OH stretch of one single HDO molecule in a system of D_2O molecules. Our results indicate that the water structures forming in pores of various diameters can be distinguished based on their specific signatures in infrared absorption spectra. In particular, we have shown that the infrared spectrum of the OH stretch in single-file water chains inside (6,6) carbon nanotubes displays a characteristic two-peak structure related to the two distinct configurations in which the OH bond can occur. Whereas in the dangling configuration the vibrational frequency is close to the frequency of the undisturbed oscillator, strong interactions with neighboring molecules lead to a red shift of the frequency in the hydrogen-bonded configuration. The spectra of single-file water are distinctly different from the spectra of stacked-ring structures forming in slightly wider carbon nanotubes[26] and also of bulk water.[19] Therefore, vibrational spectroscopy provides a way to probe experimentally the particular structure of single-file water observed only in computer simulations so far.

As in bulk water,[32] non-Condon effects play a major role for the infrared spectra of single-file water chains in nanopores. Because of the strong dependence of the transition dipole on the local molecular structure, the high-frequency peak associated with the dangling position of the OH oscillator is strongly suppressed with respect to the low-frequency peak corresponding to hydrogen-bonded configurations. Because in contrast with the transition dipole the isotropic transition polarizability

displays a much smaller variation[20,21] between different local environments, Raman spectra of nanopore water should be affected to a lesser degree by non-Condon effects such that Raman experiments could provide a more pronounced signature of the distinct populations of OH oscillators expected in these systems. Analogous effects have been observed in the Raman spectra of methanol/CCl_4[49] and methanol/acetone[50] mixtures, in which an additional line appeared with increased methanol dilution in the band of the OH stretching mode of the methanol molecule. As indicated by molecular dynamics simulation, this line originates from methanol molecules with dangling OH bond at the end of hydrogen-bonded methanol chains.

Our simulation results also confirm, for nanopore water, the previous finding[19−21] that the spectroscopic response of an HDO molecule in D_2O is mainly determined by the electric field fluctuations at the position of the hydrogen atom. The electric field acting on the hydrogen charge in the direction of the OH bond essentially determines its vibrational frequency such that the OH stretch vibration probes the charge distribution in the immediate vicinity of the hydrogen atom.[19,25]

■ ACKNOWLEDGMENT

We thank Georg Menzl and Jürgen Köfinger for useful discussions. The simulations presented in this Article were carried out on the Vienna Scientific Cluster (VSC). We acknowledge support from the Austrian Science Fund under grant W004.

■ REFERENCES

(1) Hummer, G.; Rasaiah, J. C.; Noworyta, J. P. *Nature* **1998**, *414*, 188–190.
(2) Cambré, S.; Schoeters, B.; Luyckx, S.; Goovaerts, E.; Wenseleers, W. *Phys. Rev. Lett.* **2010**, *104*, 207401.
(3) Holt, J. K.; Park, H. G.; Wang, Y.; Stadermann, M.; Artyukhin, A. B.; Grigoropoulos, C. P.; Noy, A.; Bakajin, O. *Science* **2007**, *312*, 1034–1037.
(4) Whitby, M.; Quirke, N. *Nat. Nanotechnol.* , **2007**, *2*, 87–94.
(5) Dellago, C.; Naor, M. M.; Hummer, G. *Phys. Rev. Lett.* **2003**, *90*, 105902.
(6) Koga, K.; Gao, G. T.; Tanaka, H.; Zeng, X. C. *Nature* , **2001**, *412*, 802–805.
(7) Takaiwa, D.; Hatano, I.; Koga, K.; Tanaka, H. *Proc. Natl. Acad. Sci. U.S.A.* **2008**, *105*, 39–43.
(8) Noy, A.; Park, H. G.; Fornasiero, F.; Holt, J. K.; Grigoropoulos, C. P.; Bakajin, O. *Nano Today* **2007**, *2*, 22–29.
(9) Kalra, A.; Garde, S.; Hummer, G. *Proc. Natl. Acad. Sci. U.S.A.* **2003**, *100*, 10175–10180.
(10) Hille, B. *Ion Channels in Excitable Membranes*; Sinauer Associates: Sunderland, MA, 2001.
(11) Zhu, F.; Schulten, K. *Biophys. J.* **2003**, *85*, 236–244.
(12) Alexiadis, A.; Kassinos, S. *Chem. Rev.* **2008**, *108*, 5014–5034.
(13) Hennrich, F.; Arnold, K.; Lebedkin, S.; Quintilla, A.; Wenzel, W.; Kappes, M. M. *Phys. Status Solidi* **2007**, *244*, 3896–3900.
(14) Quintilla, A.; Hennrich, F.; Lebedkin, S.; Kappes, M. M.; Wenzel, W. *Phys. Chem. Chem. Phys.* **2010**, *12*, 902–908.
(15) Köfinger, J.; Dellago, C. *Phys. Rev. Lett.* **2009**, *103*, 080601.
(16) Köfinger, J.; Dellago, C. *Phys. Rev. B* **2010**, *82*, 205416-1–205416-14.
(17) Köfinger, J.; Dellago, C. *New J. Phys.* **2010**, *12*, 093044.
(18) Köfinger, J.; Hummer, G.; Dellago, C. *Proc. Natl. Acad. Sci. U.S.A.* **2008**, *105*, 13218–13222.
(19) Eaves, J. D.; Tokmakoff, A.; Geissler, P. L. *J. Phys. Chem. A* **2005**, *109*, 9424–9436.
(20) Corcelli, S. A.; Skinner, J. L. *J. Phys. Chem. A* **2005**, *109*, 6154–6165.
(21) Auer, B.; Kumar, R.; Schmidt, J. R.; Skinner, J. L. *Proc. Natl. Acad. Sci. U.S.A.* **2007**, *104*, 14215–14220.
(22) Auer, B. M.; Skinner, J. L. *J. Chem. Phys.* **2008**, *128*, 224511.
(23) Bakker, H. J.; Skinner, J. L. *Chem. Rev.* **2010**, *110*, 1498–1517.
(24) Hayashi, T.; la Cour Jansen, T.; Zhuang, W.; Mukamel, S. *J. Phys. Chem. A* **2005**, *109*, 64–84.
(25) Smith, J. D.; Saykally, R. J.; Geissler, P. L. *J. Am. Chem. Soc.* **2007**, *129*, 13847–13856.
(26) Byl, O.; Liu, J.-C.; Wang, Y.; Yim, W.-L.; Johnson, J. K.; Yates, J. T. *J. Am. Chem. Soc.* **2006**, *128*, 12090–12097.
(27) Reimers, J. R.; Watts, R. O. *Mol. Phys.* **1984**, *52*, 357–381.
(28) Watson, I. A.; Henry, B. R.; Ross, I. G. *Spectrochim. Acta, Part A* **1981**, *37*, 857–865.
(29) Zwanzig, R. *Nonequilibrium Statistical Mechanics*; Oxford University Press: New York, 2001.
(30) Mukamel, S. *Principles of Nonlinear Optical Spectroscopy*; Oxford University Press: New York, 1998.
(31) Whalley, E.; Klug, D. D. *J. Chem. Phys.* **1986**, *84*, 78.
(32) Schmidt, J. R.; Corcelli, S. A.; Skinner, J. L. *J. Chem. Phys.* **2005**, *123*, 044513.
(33) Li, F.; Skinner, J. L. *J. Chem. Phys.* **2010**, *132*, 204505.
(34) Loparo, J. J.; Fecko, C. J.; Eaves, J. D.; Roberts, S. T.; Tokmakoff, A. *Phys. Rev. B* **2004**, *70*, 180201.
(35) Fecko, C. J.; Loparo, J. J.; Roberts, S. T.; Tokmakoff, A. *J. Chem. Phys.* **2005**, *122*, 054506.
(36) Verlet, L. *Phys. Rev.* **1967**, *159*, 98–103.
(37) Berendsen, H. J. C.; Grigera, J. R.; Straatsma, T. P. *J. Phys. Chem.* **1987**, *91*, 6269–6271.
(38) Ryckaert, J.-P.; Ciccotti, G.; Berendsen, H. J. C. *J. Comput. Phys.* **1977**, *23*, 327–341.
(39) Hummer, G., NIH, Bethesda (2003).
(40) Striolo, A.; Chialvo, A. A.; Gubbins, K. E.; Cummings, P. T. *J. Chem. Phys.* **2005**, *122*, 234712.
(41) Mikami, F.; Matsuda, K.; Kataura, H.; Maniwa, Y. *ACS Nano* **2009**, *3*, 1279–1287.
(42) Best, R. B.; Hummer, G. *Proc. Natl. Acad. Sci. U.S.A.* **2005**, *102*, 6732–6737.
(43) Mukherjee, B.; Maiti, P. K.; Dasgupta, C.; Sood, A. K *J. Phys. Chem. B* **2009**, *113*, 10322–10330.
(44) Luzar, A.; Chandler, D. *Nature* **1996**, *379*, 55–57.
(45) Luzar, A.; Chandler, D. *Phys. Rev. Lett.* **1996**, *76*, 928–931.
(46) Köfinger, J.; Dellago, C. *J. Phys. Chem. B* **2008**, *112*, 2349–2356.
(47) Fecko, C. J.; Eaves, J. D.; Loparo, J. J.; Tokmakoff, A.; Geissler, P. L. *Science* **2003**, *301*, 1698–1702.
(48) Maniwa, Y.; Matsuda, K.; Kyakuno, H.; Ogasawara, S.; Hibi, T.; Kadowaki, H.; Suzuki, S.; Achiba, Y.; Kataura, H. *Nat. Mater.* **2007**, *6*, 135–141.
(49) Musso, M.; Torii, H.; Ottaviani, P.; Asenbaum, A.; Giorgini, M. G. *J. Phys. Chem. A* **2002**, *106*, 10152–10161.
(50) Musso, M.; Giorgini, M. G.; To, H. *J. Mol. Liq.* **2009**, *147*, 37–44.